Appl. Phys. B 51, 272–284 (1990)

Applied Physics B Photophysics and Laser Chemistry

Mode Structure of Hollow Dielectric Waveguide Lasers*

J. Henningsen, M. Hammerich, and A. Olafsson**

Physics Laboratory, H.C. Ørsted Institute, Universitetsparken 5, DK-2100 Copenhagen Ø, Denmark

Received 5 February 1990/Accepted 14 May 1990

Abstract. The mode structure of hollow dielectric waveguide lasers with free space sections and flat mirrors is studied theoretically and experimentally. The study covers the fundamental mode and the three most important higher order modes, and graphs are given which identify regions of high mode discrimination in the parameter space. Calculated coupling losses are verified experimentally by detailed studies of the output power of CO_2 lasers as a function of resonator geometry. The intensity profile inside and outside the resonator is calculated, and the profile outside the resonator is compared with experiments for the fundamental mode as well as for the higher order modes. It is shown that in general the fundamental mode is non-Gaussian, and that drastically different output characteristics are obtained for different choice of output plane. The paper identifies design criteria for obtaining single line and single mode oscillation over a wide tuning range, even in the densest region of the CO_2 laser line spectrum, and this is exemplified by a spectroscopic application.

PACS: 42.55D, 42.60B, 42.60D, 42.80L

Hollow dielectric waveguides are widely used for small CO_2 lasers, mainly because they allow for compact designs with a large optical output per unit discharge volume [1]. Although their potential for yielding a large tunability in a given laser line by using short resonators with a large free spectral range was also recognized at an early stage, this feature has generally been less emphasized in the subsequent development [2]. One reason for this may be that tunability is relevant to a rather specialized use of the laser only, but it may also be due to the notorious difficulty in maintaining single line and single mode operation over the entire free spectral range of a short laser. Most waveguide lasers are optimized with respect to output power by placing the end reflectors as close to the waveguide as possible. However, in that case there is only little loss discrimination between the fundamental mode and higher order modes, and it is very difficult to avoid mode jumping as the frequency is tuned away from the center of the gain profile. The required loss discrimination can be obtained through propagation losses, by using narrow bore waveguides, but then the resolution of the grating suffers, and unless intra cavity elements are used in order to expand the laser beam, it becomes difficult to obtain single line operation in the densest regions of the CO_2 laser line spectrum. In this paper we shall discuss the mode properties of short hollow dielectric waveguide lasers with special emphasis on the requirements for single mode operation over a wide tuning range through coupling loss discrimination.

A waveguide laser resonator basically consists of a piece of waveguide with a reflector at each end. For practical reasons it will usually not be possible to terminate the waveguide with the reflectors, and the laserbeam will then experience regions of free space propagation inside the resonator. The electromagnetic modes of a hollow dielectric waveguide with circular cross section were determined by Marcatili and Schmeltzer in 1964 [3]. Whenever such a single mode leaves the waveguide, it will couple into a superposition of free space modes, and the resulting field configuration will propagate with a divergence angle essentially given by λ/a, where λ is the free space wavelength, and a is the waveguide radius. Thus, if a flat reflector is used, some radiation will inevitably be lost when the beam reenters the waveguide, and this coupling loss will increase monotonically with the distance between reflector and

* Supported by the Danish Science Research Councils under grants no. 5.17.4.6.19 and 5.17.4.1.23 and by FLS airloq

** Present address: Science Institute, University of Iceland, Dunhaga 3, 107 Reykjavik, Iceland

waveguide. To minimize this loss, the conventional approach is to either place the reflector as close to the guide as possible, or to use a curved reflector in order to refocus the beam at the waveguide entrance [4].

The first to point out the importance of using linear combinations of waveguide modes for achieving transverse mode control in waveguide lasers with spherical mirrors were Roullard and Bass [5], and this was applied to CO_2 lasers by Lyszyk et al. [6], who studied a laser resonator terminated by a flat grating and a spherical mirror. However, it was noted by Jensen and Tobin [7] that even when using two flat reflectors, there would occasionally be a range where the laser output would actually increase with increasing separation between waveguide and reflector, indicating a local loss minimum at a specific separation. In 1984, Gerlach et al. [8] analyzed this situation for waveguides with circular cross section, and found that this loss minimum had a straightforward physical interpretation. Owing to the presence of free space regions, the eigenmodes of the actual resonator cannot be pure waveguide modes. Assuming instead a linear combination of low order modes, they found that for a symmetric resonator, the location of the loss minimum corresponds to the fulfillment of a phase condition, such that the phase difference between the EH_{11} and EH_{12} modes increases by 2π during a single pass of the resonator. In this way the relative phases can adjust such that each time the two modes reenter the waveguide, they interfere destructively at the edge, and constructively at the center, leading to a resulting field which is more confined along the axis than the pure EH_{11} mode, and hence couples better into the waveguide.

Since practical lasers usually employ polarizing components, such as Brewster windows or diffraction gratings, the theoretical analysis was confined to waveguide modes with linear polarization, and circularly symmetric intensity distribution, i.e. EH_{1m} modes with $m=1,2,3,\ldots$. They found that for a symmetric resonator loss minima will exist whenever the condition

$$\frac{L}{ka^2} \simeq \frac{4p\pi}{u_{1m}^2 - u_{11}^2} \qquad p=1,2,3,\ldots,\ m=2,3,\ldots \tag{1}$$

is satisfied, where L is the total resonator length, k is the free space wavenumber, a is the guide radius, and u_{1m} is the mth zero of the zero-order Bessel function J_0. For an asymmetric resonator the number of loss minima will be doubled, and if the waveguide is terminated with a reflector at one end, loss minima will correspond to half-integral values of p, since the resonator is then equivalent to a symmetric resonator with length $2L$. Gerlach et al. verified their theoretical findings by determining the location of the $m=2$, $p=1$ output power maximum for symmetric resonators with a range of different resonator lengths using alumina waveguides with diameter 2.4 mm. They considered the fundamental mode only, and they found very good agreement with (1), although the experimentally determined optimum resonator lengths tended to be slightly larger than predicted theoretically.

In order to optimize tunability, it is advantageous to work with asymmetric resonators, since they allow for loss minima at smaller values of L. In addition, if single mode operation is important, it is necessary to study also the higher order modes. Although the basis of three EH_{1m} modes used by Gerlach et al. yields three solutions, we shall show that these are in fact not the three linearly polarized modes with lowest loss, and that other modes have to be taken into account. In the following, we first outline the theory, and for the relevant modes of an asymmetric resonator, we calculate the coupling loss as a function of separation between one reflector and the waveguide. The calculated coupling losses are used as input into the Rigrod model of high gain lasers [9], and the resulting output curves are compared with the measured output of a series of grating controlled pyrex waveguide lasers with different waveguide length and diameter, and different operating frequencies. Graphs are given, which show the field distribution inside and outside the resonator for the lowest order modes, and results for the far field are compared with experiment.

1. Theory

In this section, we outline the theory, which closely follows that developed by [8]. The resonator is unfolded as shown in Fig. 1, and the field at position 1 is expressed as a superposition of waveguide modes. Each of these modes is expanded in a basis of free space modes with a suitably chosen beamwaist w_0, located at the exit plane of the waveguide, and these modes next undergo free space propagation with the appropriate phase development over a distance $2D_1$. When reentering the waveguide, the beamwaist and the phase front radius of curvature have evolved to

$$w = w_0\sqrt{1+\left(\frac{2D_1\lambda}{\pi w_0^2}\right)^2}, \tag{2}$$

$$R = z\left[1+\left(\frac{\pi w_0^2}{2D_1\lambda}\right)^2\right]. \tag{3}$$

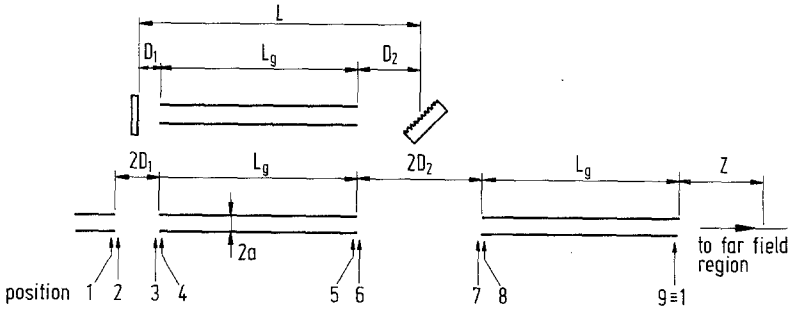

Fig. 1. Schematic diagram of resonator and unfolded resonator

Rather than projecting directly back upon the waveguide basis, the free space modes are first transformed to a different free space basis with beamwaist w_0 and flat phase fronts, and the advantage now is that the further transformation to the waveguide basis is just the inverse of the initial transformation out of this basis at position 1. The waveguide modes next propagate in the waveguide and acquire loss and phase shift as determined by [3]. The free space region $2D_2$ is treated as $2D_1$, and after a final pass through the waveguide, the field is back where it started. Each of these steps can be expressed in terms of a complex matrix operating on the basis functions, and by matrix multiplication we arrive at a resulting transformation matrix which expresses the development of the field during one double pass of the resonator. Equating this to a complex constant multiplied by the initial field, an eigenvalue equation results which, when diagonalized, yields the eigenvalues and eigenvectors. Writing the complex eigenvalue as $|\lambda|\exp(i\phi)$, the round trip loss is given by $1-|\lambda|^2$, while ϕ determines the relative phase shifts of the different eigensolutions.

When carrying out this procedure, three decisions have to be made: the size of the waveguide basis, the size of the free space basis, and the value of w_0 used for the free space basis. As for the waveguide basis, we first adopt the same criterion as [8], that only modes with linear polarization are considered, and we choose the polarization to be along the y-axis, so that $E_y = E_r \sin\theta + E_\theta \cos\theta$. The modes may be classified according to the number of azimuthal nodal planes for the electric field, and the first class, with no nodal planes, contains the hybrid modes EH_{1m}. In the limit $ka \gg 1$, and excluding regions very close to the waveguide wall, the normalized electric field is given by

$$\phi = \frac{1}{\sqrt{\pi}\,|J_1(u_{1m})|a} J_0\left(u_{1m}\frac{r}{a}\right) \qquad r \leqq a,\ m=1,2,\ldots, \tag{4}$$

where u_{nm} is the mth zero of $J_{n-1}(x)$, and normalization implies

$$\int_0^{2\pi}\int_0^a \phi^2 r\,dr\,d\theta = 1. \tag{5}$$

The intensity distribution is cylindrically symmetric, with a maximum at the center, and $m-1$ zeros between the center and the waveguide wall. The EH_{11} mode has the lowest propagation loss of all possible waveguide modes, and it is thus natural to assume that the lowest order mode of the actual waveguide is a linear combination of EH_{1m} modes, dominated by EH_{11}. This was the basis used by [8], and they used up to three modes in their analysis.

When the EH_{1m} modes couple into free space, they predominantly excite the $TEM^{(0)}_{m-1}$ modes with normalized electric field given by

$$\psi^{(0)}_{m-1} = \sqrt{\frac{2}{\pi}}\frac{1}{w_0}\mathscr{L}^{(0)}_{m-1}\left(\frac{2r^2}{w_0^2}\right)\exp\left(-\frac{r^2}{w_0^2}\right), \tag{6}$$

where $\mathscr{L}$ is an associated Laguerre polynomial, defined through the expansion

$$\mathscr{L}^{(\alpha)}_p(x) = \sum_{m=0}^{p}(-1)^m\frac{(\alpha+p)!}{(p-m)!(\alpha+m)!}\frac{x^m}{m!}, \tag{7}$$

and normalization implies

$$\int_0^{2\pi}\int_0^\infty \psi^2 r\,dr\,d\theta = 1. \tag{8}$$

By a suitable choice of w_0, the coupling can be optimized for each m individually, and the traditional value of $w_0 = 0.6435a$, given by [10], corresponds to an optimum coupling of 98% from EH_{11} into $TEM^{(0)}_0$. For higher order modes, optimum coupling is obtained for a smaller value of w_0. We have chosen to work with basis of 4 EH_{1m} modes and 7 $TEM^{(0)}_m$ modes, and with this choice we have found $w_0 = 0.4a$ to be suitable.

The second class, containing modes with one azimuthal nodal plane, consists of the composite modes

$$TE_{0m} + EH_{2m}, \quad m=1,2,\ldots,$$
$$TM_{0m} + EH_{2m}, \quad m=1,2,\ldots.$$

In the limit $ka \gg 1$, the electric field of these modes is given by

$$TE_{0m}: \begin{cases} E_\theta = J_1\left(u_{0m}\dfrac{r}{a}\right) \\ E_r = 0, \end{cases} \tag{9}$$

$$TM_{0m}: \begin{cases} E_\theta = 0 \\ E_r = J_1\left(u_{0m}\dfrac{r}{a}\right), \end{cases} \tag{10}$$

$$EH_{2m}: \begin{cases} E_\theta = J_1\left(u_{0m}\dfrac{r}{a}\right)\cos 2(\theta+\theta_0) \\ E_r = J_1\left(u_{0m}\dfrac{r}{a}\right)\sin 2(\theta+\theta_0), \end{cases} \tag{11}$$

and the resulting field then becomes

$$TE_{0m}+EH_{2m}: \begin{cases} E_\theta = J_1\left(u_{0m}\dfrac{r}{a}\right)[1+\cos 2(\theta+\theta_0)] \\ E_r = J_1\left(u_{0m}\dfrac{r}{a}\right)\sin 2(\theta+\theta_0), \end{cases} \tag{12}$$

$$TM_{0m}+EH_{2m}: \begin{cases} E_\theta = J_1\left(u_{0m}\dfrac{r}{a}\right)\cos 2(\theta+\theta_0) \\ E_r = J_1\left(u_{0m}\dfrac{r}{a}\right)[1+\sin 2(\theta+\theta_0)], \end{cases} \tag{13}$$

where θ_0 is an arbitrary constant, specifying the orientation of the nodal plane. Polarization along the y-axis corresponds to $\theta_0 = 0$ for $TE_{0m}+EH_{2m}$, and $\theta_0 = -\pi/4$ for $TM_{0m}+EH_{2m}$, and the corresponding normalized electric fields are

$$TE_{0m}+EH_{2m}: \phi = \frac{1}{a}\sqrt{\frac{2}{\pi}}\frac{1}{|J_2(u_{2m})|}J_1\left(u_{2m}\frac{r}{a}\right)\cos\theta, \tag{14}$$

$$TM_{0m}+EH_{2m}: \phi = \frac{1}{a}\sqrt{\frac{2}{\pi}}\frac{1}{|J_2(u_{2m})|}J_1\left(u_{2m}\frac{r}{2}\right)\sin\theta. \tag{15}$$

When leaving the waveguide, these modes predominantly excite the free space modes $TEM^{(1)}_{m-1}$, with normalized

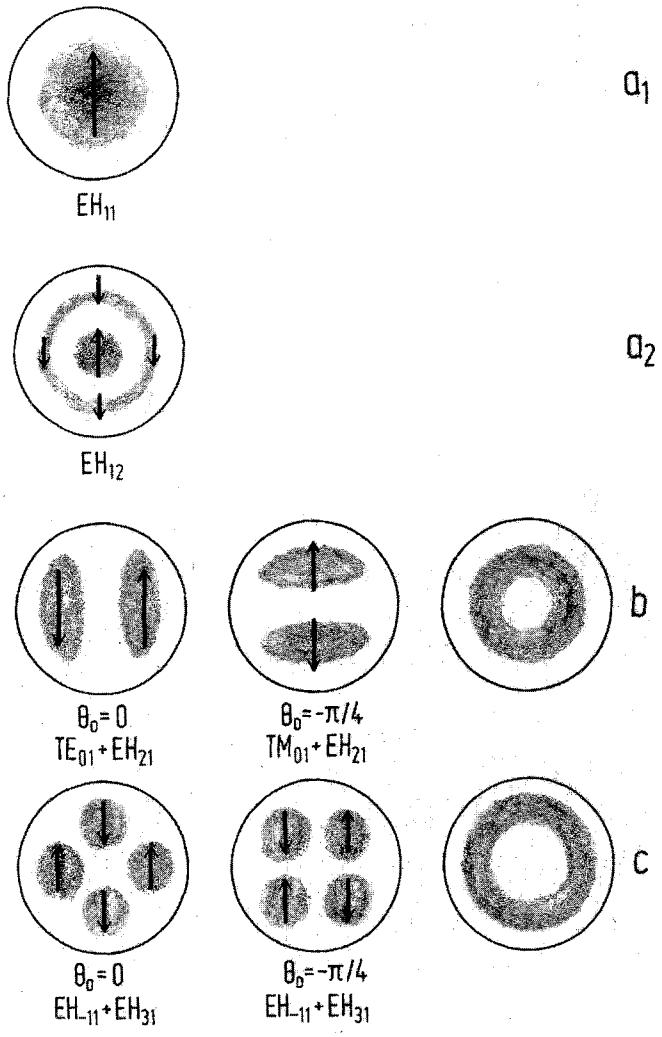

Fig. 2a–c. Intensity patterns for linearly polarized hollow dielectric waveguide modes with zero (**a**), one (**b**), and two (**c**) azimuthal nodal planes

electric field given by

$$\psi_{m-1}^{(1)} = \sqrt{\frac{4}{\pi}}\frac{1}{m}\sqrt{2}\frac{r}{w_0}\mathscr{L}_{m-1}^{(1)}\left(\frac{2r^2}{w_0^2}\right)\exp\left(-\frac{r^2}{w_0^2}\right)\begin{cases}\cos\theta\\ \sin\theta.\end{cases} \quad (16)$$

The field configurations for the composite modes with $m=1$ are shown in Fig. 2b. Since for each m the two nearly degenerate modes are mutually orthogonal, they may be excited independently of one another. If they are excited simultaneously, the intensity distribution becomes circularly symmetric, and for $m=1$ this produces the well-known ring-shaped doughnut pattern.

The last class which we shall consider, contains modes with two nodal planes. The waveguide basis consists of the combinations

$$\mathrm{EH}_{-1m}+\mathrm{EH}_{3m} \qquad m=1,2,\ldots$$

which for $\theta_0=0$ and $\theta_0=-\pi/4$ yields the mutually orthogonal normalized electric fields

$$\phi = \frac{1}{a}\sqrt{\frac{2}{\pi}}\frac{1}{|J_3(u_{3m})|}J_2\left(u_{3m}\frac{r}{a}\right)\begin{cases}\cos 2\theta\\ \sin 2\theta.\end{cases} \quad (17)$$

Their free space counterparts are $\mathrm{TEM}_{m-1}^{(2)}$, with normalized electric field given by

$$\psi_{m-1}^{(2)} = \frac{1}{a}\sqrt{\frac{4}{\pi}}\sqrt{\frac{1}{m(m+1)}}2\frac{r^2}{w_0^2}\mathscr{L}_{m-1}^{(2)}\left(2\frac{r^2}{w_0^2}\right) \times\exp\left(-\frac{r^2}{w_0^2}\right)\begin{cases}\cos 2\theta\\ \sin 2\theta.\end{cases} \quad (18)$$

The field configurations for $m=1$ are shown in Fig. 2c. If the two modes are excited separately, they give rise to a four-clover intensity pattern, and if they are excited simultaneously with the same amplitude, the intensity distribution again turns into a circularly symmetric doughnut pattern, but with a larger diameter.

Owing to their different angular dependence, modes of different classes are mutually orthogonal both in the waveguide and in free space, and since for a cylindrically symmetric resonator there is no mixing, they can be treated completely independent of one another. Since we are concerned with the higher order modes only in sofar as they represent a threat to single fundamental mode operation of the laser, we have restricted the waveguide basis for modes with azimuthal nodal planes to modes with $m=1$ and 2, and used only 5 free space modes with $w_0=0.5a$.

The phase shift acquired by the $\mathrm{TEM}_p^{(\alpha)}$ mode over a distance z in the free space region, is given by

$$\exp\left[-\mathrm{i}(2p+\alpha)\arctan\frac{2z'}{(w_0/a)^2}\right], \quad (19)$$

where $z'=z/ka^2$, and the phase is measured relatively to the $\mathrm{TEM}_0^{(0)}$ phase. The loss and phase shift acquired by a waveguide mode $(\ )_{nm}$ in a waveguide of length L_g and radius a, is given by

$$\exp[-u_{nm}^2 l_g\,\mathrm{Re}\{v_n'\}]\exp\left[-\frac{\mathrm{i}}{2}(u_{nm}^2-u_{11}^2) \times l_g(1+2\,\mathrm{Im}\{v_n'\})\right], \quad (20)$$

where $l_g=L_g/ka^2$ *and* $v_n'=v_n/ka$. v_n is given by

$$v_n=\begin{cases}\dfrac{1}{\sqrt{v^2-1}}\ \mathrm{TE}_{0m}\ \text{modes}\\ \dfrac{v^2}{\sqrt{v^2-1}}\ \mathrm{TM}_{0m}\ \text{modes}\\ \dfrac{v^2+1}{2\sqrt{v^2-1}}\ \mathrm{EH}_{nm}\ \text{modes},\end{cases} \quad (21)$$

where v is the complex refractive index of the dielectric. The phase shifts are measured relatively to the EH_{11} phase, and the constants u_{nm} are given in Table 1.

It follows from above that all transformations can be expressed in terms of the dimensionless parameters $l_g=L_g/ka^2$, $d_1=D_1/ka^2$, $d_2=D_2/ka^2$, $l=L/ka^2$, and $v_n'=v/ka$. With a real refractive index of 1.5, the three values of v_n are 0.894, 2.010, and 1.453 respectively. For our range of experimental conditions we have $ka\simeq 1000$ and $l_g\leqq 0.25$, so that propagation losses in the waveguide

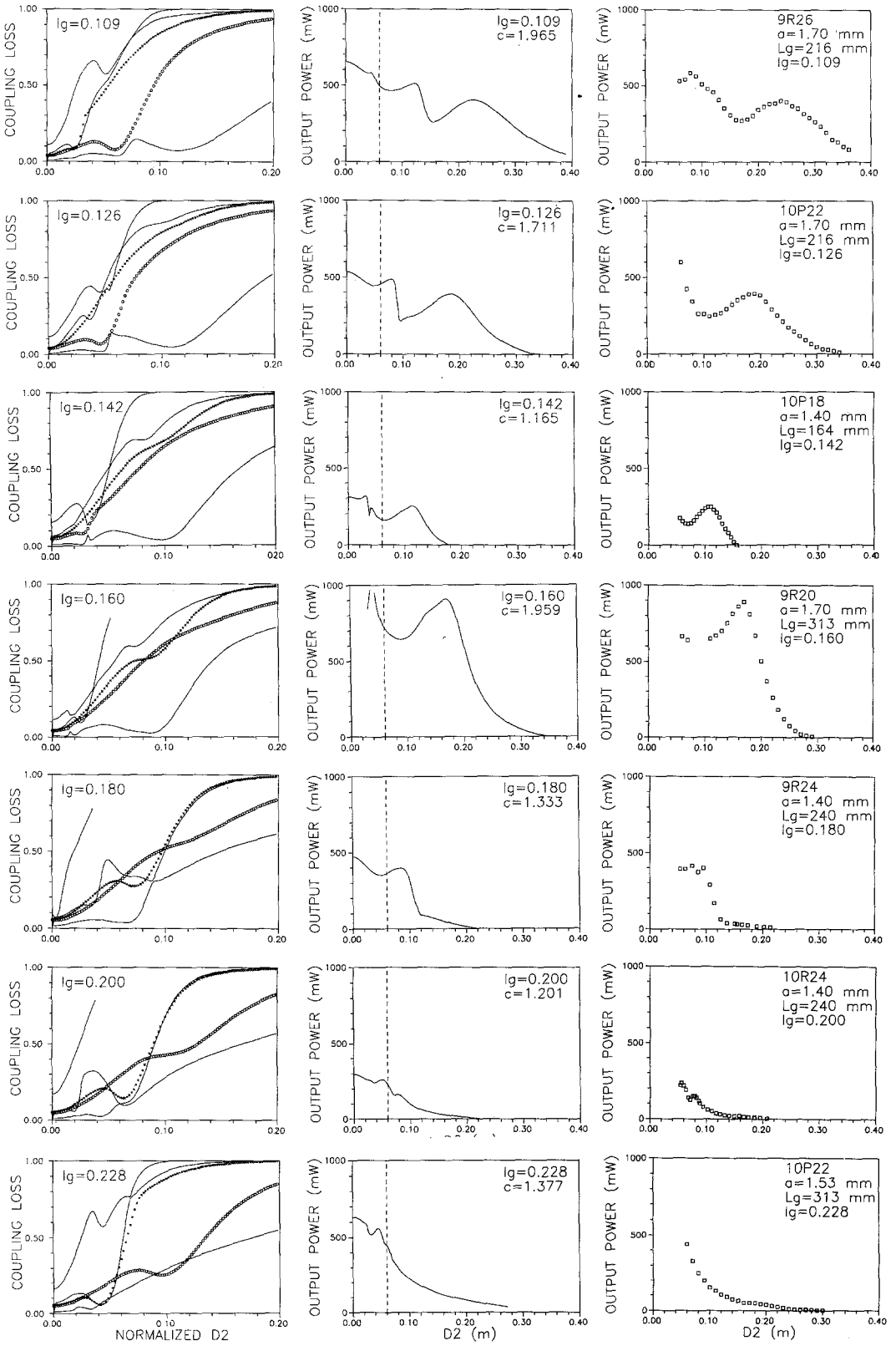

Fig. 3. First column: Calculated coupling loss vs d_2 for seven different normalized waveguide lengths l_g ($d_2 = D_2/c$ and $d_1 = 0.015/c$, where $c \equiv ka^2$ is given in the graphs of second column). Full lines refer to the three lowest order modes with zero azimuthal nodal planes, open circles to the lowest order mode with one, and crosses to the lowest order mode with two azimuthal nodal planes. Second column: Calculated output power for lasers with normalized waveguide lengths corresponding to the first column, but using $D_2 = cd_2$ as independent variable. The dotted line indicates the minimum value of D_2 allowed by the experimental arrangement. Third column: Measured average output for the lasers of the second column

Table 1. mth zero of $(n-1)$th order Bessel function

n,m	1	2	3	4
1	2.405	5.520	8.654	11.792
2,0	3.832	7.016	10.173	13.324
3, −1	5.136	8.417	11.620	14.796

Table 2. Normalized resonator length corresponding to loss minima for two-mode interference

p	1	2	3	4
EH_{11}/EH_{12}	0.255	0.509	0.764	1.018
EH_{11}/EH_{13}	0.091	0.182	0.273	0.364
EH_{11}/EH_{14}	0.047	0.094	0.141	0.189
EH_{12}/EH_{13}	0.141	0.283	0.424	0.566
EH_{12}/EH_{14}	0.058	0.116	0.174	0.231
EH_{13}/EH_{14}	0.098	0.196	0.294	0.392
EH_{21}/EH_{22}	0.182	0.364	0.546	0.728
EH_{31}/EH_{32}	0.141	0.283	0.424	0.565

are insignificant. We may therefore neglect effects related to the refractive index, and in all calculations we have used $\nu_n'=0.001$.

Although the actual resonator modes are linear combinations of pure waveguide modes, they are usually dominated by a single component, and this component may then be used for designating the particular resonator mode. Close to the local loss minima, there are significant contributions from other waveguide modes, and here we therefore include the dominant interfering mode in the designation. For waveguide modes with one or more azimuthal nodal planes, the linearly polarized combinations always contain a hybrid mode component of the type EH_{nm}, where $n>0$, and this component will be used for designating the particular combination.

Figure 3 shows the coupling loss as a function of d_2 for fixed d_1 and 7 different values of l_g, varying from 0.109 to 0.228. The location of mode mixing minima according to the condition (1) are given in Table 2 and with $l=l_g+d_1+d_2$ it is straightforward to identify the local minima of the loss curves. Starting with $l_g=0.109$, we first notice the strong EH_{11}/EH_{12} minimum at $d_2=0.115$, with a coupling loss of about 10% and a very good mode discrimination. Reducing d_2, the EH_{11}/EH_{13} minimum for $p=2$ appears at $d_2\simeq 0.06$. Here, however, the EH_{21}/EH_{22} doughnut mode has its first loss minimum as well, and improved mode discrimination can be achieved at the expense of a moderate increase in coupling loss, by further reducing d_2 to about 0.04. As l_g increases, the loss pattern moves inwards, so that the total resonator length corresponding to a given feature remains essentially constant. For $l_g>0.170$, the EH_{11}/EH_{13} minimum moves into the waveguide, and at the same time two new features appear. For $l_g=0.200$ we observe loss minima corresponding to EH_{12}/EH_{13} mixing at $d_2\simeq 0.065$ and mixing of the EH_{31}/EH_{32} modes at roughly the same d_2. Finally, at $l_g=0.228$, we observe the second EH_{21}/EH_{22} doughnut minimum at $d_2\simeq 0.10$, while the EH_{31}/EH_{32} minimum at $d_2\simeq 0.04$ dips down below the fundamental mode.

2. Experiment

The findings illustrated in Fig. 3 have been studied experimentally through a series of measurements on pyrex waveguide lasers with different combinations of diameter in the range 2.8 to 3.5 mm and length in the range 160 to 313 mm, and through operation from 9.2 to 10.8 μm. The general design of our laser has been reported previously [11], and only minor modifications to enable easier exchange of waveguide have been introduced. At one end the resonator is terminated by an internal, flat ZnSe mirror whose reflectivity varies between 96 and 98% over the CO_2 laser bands. At the other end, the waveguide is terminated by a ZnSe Brewster window, and the resonator is terminated by a flat, Littrow mounted grating with 150 lines/mm. The gas is a 64/18/18% mixture of $He/N_2/CO_2$, and is flowed at a rate between 100 and 200 ml/min STP, while the pressure in the waveguide varies between 80 and 120 Torr, depending on the waveguide dimensions. The laser is excited by a pulsed power supply with 10 μs pulses at a repetition rate of 600–800 Hz.

The calculated coupling losses are used as input in the Rigrod expression [9]

$$P_{\text{out}}=P_s\frac{\sqrt{r_2}t_1}{(\sqrt{r_1}+\sqrt{r_2})(1-\sqrt{r_1r_2})}(g_0L_g+\ln\sqrt{r_1r_2}),$$

where P_s is the saturation power, g_0 the small signal gain coefficient, L_g the gain length, t_1 the transmission coefficient of the output mirror, and $r_{1,2}$ the effective power reflection coefficient at the mirror and the grating end of the resonator respectively. In the experiments, D_1 was fixed at 15 mm in order to protect the mirror, while D_2 was varied from about 60 mm, corresponding to the smallest practical separation between the grating and the waveguide, out to a maximum of 360 mm. Since D_2 is thus always much larger than D_1, the coupling losses a_c are lumped together with the grating loss of 0.05 and an assumed Brewster window loss of 0.02 to produce the effective reflectivity $r_2=0.93-a_c$. In the other end, an assumed mirror loss of 0.02 together with the mirror transmission t_1, produces the effective reflection coefficient $r_1=0.98-t_1$.

Both the gain coefficient and the saturation power depend on waveguide dimensions, pressure, flow, and discharge energy. In addition, the losses in the mirror and the Brewster window will tend to increase with the operation time of the laser, and the grating efficiency is a function of the wavelength. Rather than attempting to account for all of this, we have performed all calculations with losses as given above, with a mirror transmission $t_1=0.02$, and with a gain coefficient of $g_0=2.0\ \text{m}^{-1}$. The effect of individual variations in all of these parameters is absorbed in the saturation power, which is adjusted so as to produce agreement with experiment at the EH_{11}/EH_{12} output maximum. This

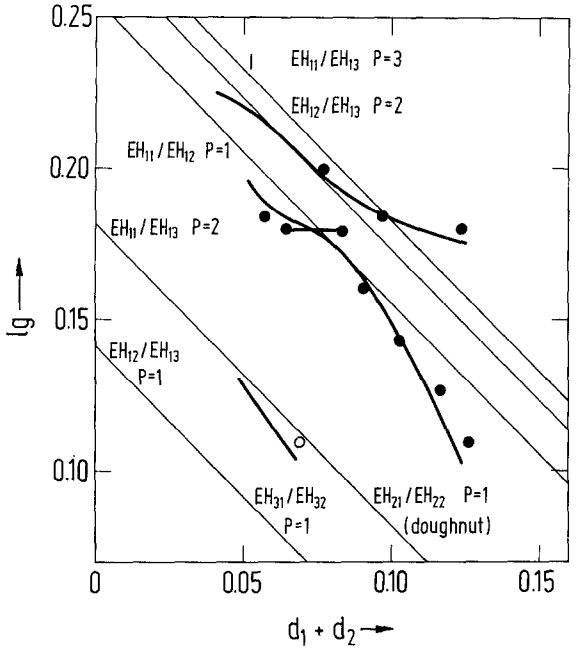

Fig. 4. Calculated and measured normalized free space length d_1+d_2 in the resonator, corresponding to loss minima for lasers with different normalized waveguide length l_g. Heavy full lines are the results of the calculations, while the thin full lines represent the predictions of simple two-mode interference as given in Table 2

procedure may be problematic close to the threshold, and may therefore affect the maximum value of D_2 for which the laser is predicted to oscillate. However, this is balanced by the fact that in this region, the coupling losses generally increase rapidly with D_2.

3. Output Power

3.1. Lowest Order Mode

In the second and third columns of Fig. 3, the calculated power for the lowest order mode is compared with experiments for the 7 values of l_g corresponding to the first column. The actual waveguide dimensions and the wavelength are shown in each experimental graph, and to give a better feeling for the actual experimental conditions, we have used D_2 rather than d_2 as independent variable. We find that the calculations reproduce all essential features of the experiments. In Fig. 4 we have compared measured and calculated values for d_2+d_1 corresponding to the local power maxima, indicating with straight lines the predictions following from Table 2. For the EH_{11}/EH_{12} maximum the agreement for L is within 2% except for $l_g=0.180$. Here, a slight change in grating adjustment would shift the maximum between the two values indicated. Note that around $l_g=0.170$ condition (1) leads to the correct L value, whereas both for higher and lower l_g, the correct L is smaller than predicted from (1). In several cases lasing persisted beyond $D_2=360$ mm, which was the maximum length allowed by our experimental setup, and it is noted that in all cases the oscillation limit for d_2 is fairly accurately predicted by the theory.

For $l_g=0.180$ and 0.200, the loss calculations indicate a mode crossing at $d_2\simeq 0.085$ and 0.060 respectively. This

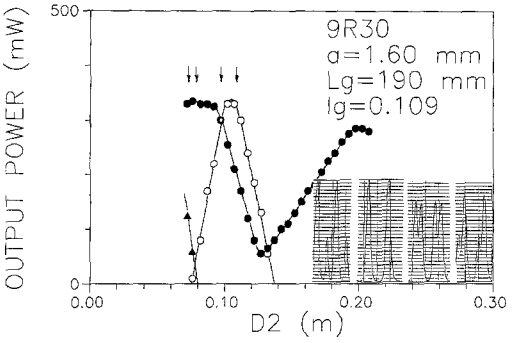

Fig. 5. Measured output power of fundamental mode (filled circles) and higher order EH_{12} doughnut mode (open circles). Inserts show photoacoustic spectra for CO_2, recorded at the location of the arrows. Triangles indicate oscillation in a neighboring line

feature is clearly seen in the experiments where it leads to a kink in the output versus D_2 graph. One feature which is not so well reproduced, is the EH_{11}/EH_{13} loss minimum for $p=2$, which according to the calculations should lead to a power maximum at $D_2\simeq 125$ mm for $l_g=0.109$, and 80 mm for $l_g=0.126$. Presumably this is related to the doughnut mode which has a loss minimum at slightly lower d_2 values, and which may contribute to the total output power in this range.

3.2. Higher Order Modes

For maximum tunability it is desirable to work at as small a D_2 as possible, and considering the lowest order mode only, this would suggest an l_g in the range 0.12 to 0.14, where the coupling losses are only about 3% for $d_2\simeq 0.05$ to 0.03, owing to the EH_{11}/EH_{13} mixing. However, as seen from Table 1 as well as from Fig. 3, this loss minimum is coincident with the loss minimum for the EH_{21} doughnut mode, which has a coupling loss of only 7%, and this will lead to very poor mode discrimination. Some improvement can be obtained by a slight reduction of d_2 to a local loss maximum for the doughnut mode. The situation is illustrated in Fig. 5, which shows the experimental power curves for both the lowest order mode and the doughnut mode, using the $l_g=0.109$ configuration. The power in the two modes was quantified by recording photoacoustic absorption in pure CO_2 at a pressure of

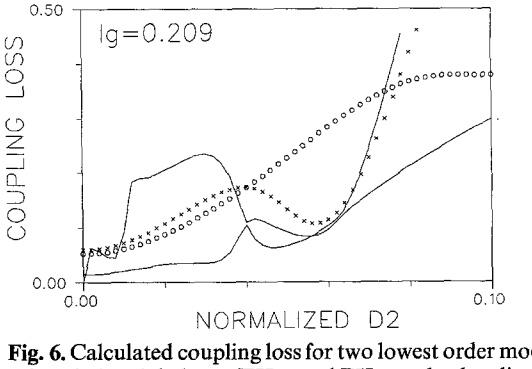

Fig. 6. Calculated coupling loss for two lowest order modes with zero azimuthal nodal planes (EH_{11} and EH_{12}-unbroken lines), for lowest order mode with one azimuthal nodal plane (EH_{21}-open circles), and two azimuthal nodal planes (EH_{31}-crosses)

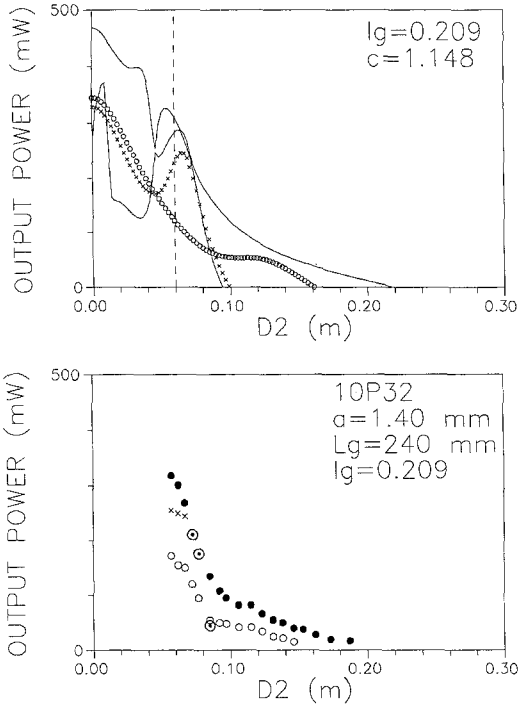

Fig. 7. Calculated output power for laser with coupling losses of Fig. 6 (upper graph), and corresponding experimental output power (lower graph). Filled circles represent the fundamental EH_{11} mode, open circles the EH_{21} doughnut mode, crosses the EH_{31} doughnut mode, and circles with a dot the EH_{12} mode

about 10 Torr, where the absorption line is essentially Doppler broadened. For single line and single mode operation, the spectrum will consist of a single line located at the center of the tuning range, while multiple peaks indicate operation in several lines or modes. Inserts in Fig. 5 show the photoacoustic signal for three different values of D_2. In each case, the line was checked by a spectrum analyzer, and the intensity pattern was checked with fluorescence plates. By fine tuning the resonator length according to [12], single line and single mode operation was achieved over the full 540 MHz tuning range at D_2 values around 80 mm. At smaller values of D_2, the laser tended to jump to a neighbouring line when tuned close to the tuning edge, as witnessed by the small photoacoustic resonance centered between the main peaks.

Other types of higher order modes can be observed for higher values of l_g, where their loss minima correspond to coupling losses of the same order of magnitude as those of the lowest order mode. They were studied for $l_g=0.209$, and in the range $d_2<0.076$ a total of 4 different modes were identified in the photoacoustic spectrum. The calculated coupling losses are shown in Fig. 6, while calculated and measured output power for these modes is shown in Fig. 7. Their identity will be further discussed in Sect. 5 below, where we are concerned with their intensity pattern in the far field region.

4. Fundamental Mode

Single fundamental mode properties were studied for $l_g=0.180$ and $d_2=0.076$, where the losses of higher order modes are sufficient to prevent oscillation (Fig. 3).

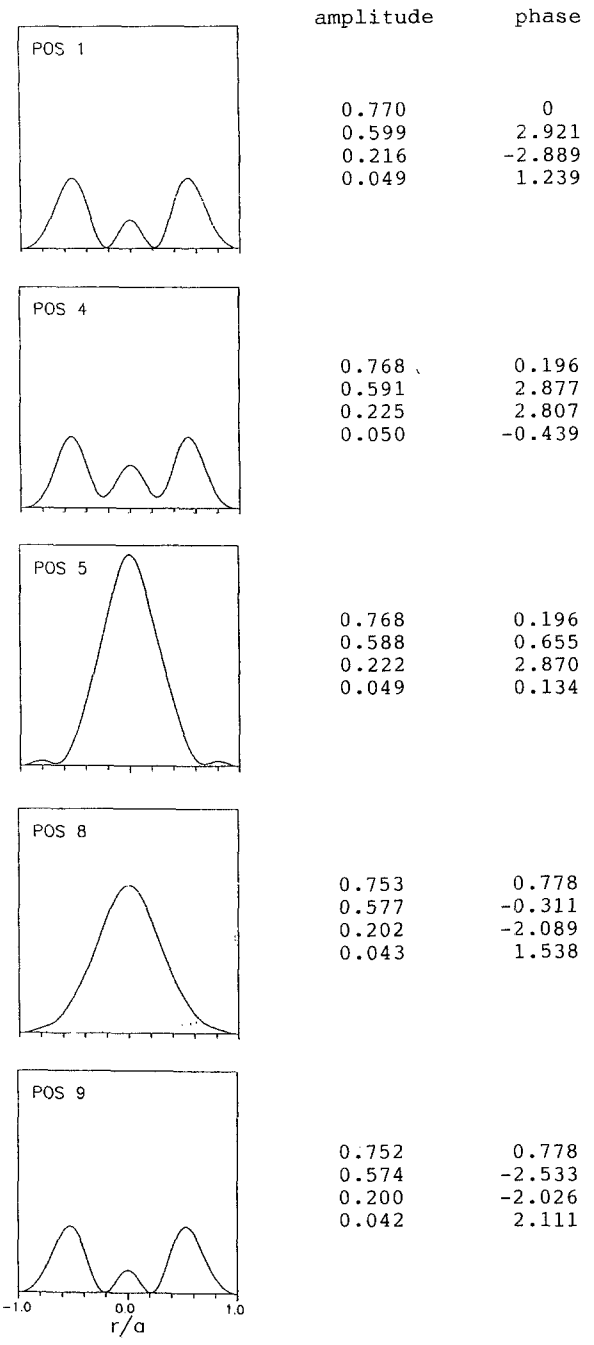

Fig. 8. Calculated intra cavity intensity profiles at five different positions in the resonator (referring to Fig. 1). Adjacent to each graph is shown amplitude and phase (modulo 2π) of the four components of the corresponding eigenvector

4.1. Intra-Cavity Intensity Profile

The intensity profile for the fundamental mode was evaluated from the appropriate eigenvector, and the results are shown in Fig. 8. The positions refer to Fig. 1, and adjacent to each figure we have given the amplitude and the phase (modulo 2π) for the four components of the eigenvector. Note that within the waveguide the phases are measured relatively to the EH_{11} phase, which remains unchanged. At position 4, where the field reenters the waveguide, the EH_{12} and EH_{13} components are both about π out of phase with EH_{11}. The resulting pattern is

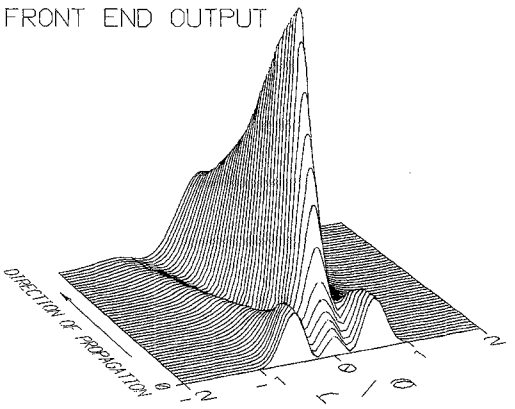

Fig. 9. Development of the intensity profile towards the far field region for output from the front end mirror. The graph extends out to a distance of 25 cm from the output plane

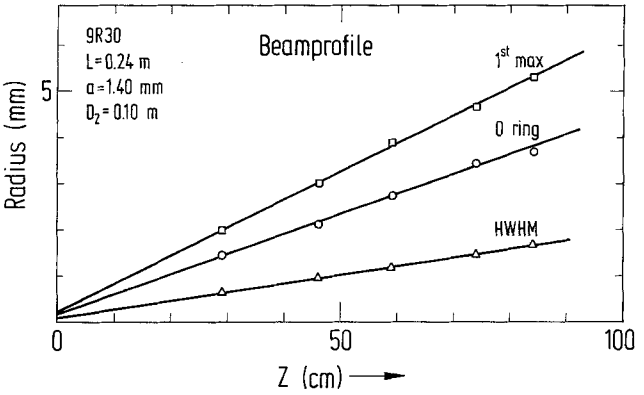

Fig. 10. Measured radii of the HWHM point of the central peak, the zero intensity ring, and the maximum intensity of the first ring, for the front end output beam of a laser with configuration as indicated

essentially ring shaped, and the necessary reduction of the field near the waveguide wall is brought about by the EH_{13} component. At position 8, where the field reenters the other end of the waveguide, EH_{11} and EH_{12} are only about $\pi/3$ out of phase, while EH_{13} is essentially in counterphase. Thus, both EH_{12} and EH_{13} interfer destructively with EH_{11} near the waveguide wall.

The net result is an intensity profile which changes drastically as the beam moves through the resonator.

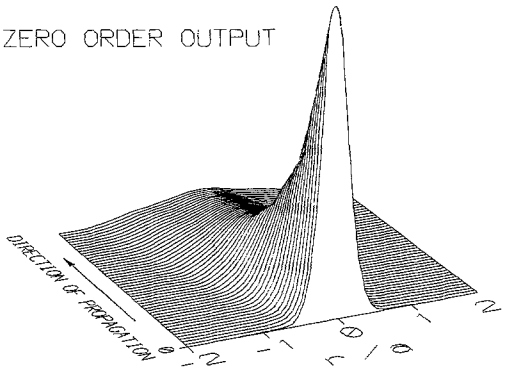

Fig. 12. Development of the intensity profile towards the far field region for zero order output beam. The graph extends from the output plane to a distance of 25 cm

Also, inspection of the profiles at positions 5 and 8 show that the two counterpropagating beams are significantly different at this end of the waveguide. The intra cavity intensity distribution cannot be probed directly without perturbing the resonator, but it reflects itself in the beam outside the resonator, which we consider in the following section.

4.2. Far Field Intensity Profile

The intensity profile outside the resonator is calculated by evaluating the eigenvector at the output coupler (position 2), and allowing the TEM modes to propagate over a suitable distance in free space before adding the fields. At position 1, the profile is very different from what is expected for a fundamental mode. However, as the beam propagates away from the laser, the profile changes, and the development towards the far field region is shown in Fig. 9.

Experimental profiles were recorded by scanning a pinhole with 120 μm diameter across the beam, and measuring the transmitted power with a large area detector with homogeneous response. Recordings were made for a number of different positions between 29 and 84 cm from the output coupler. In all cases we found a pattern qualitatively similar to that produced by diffrac-

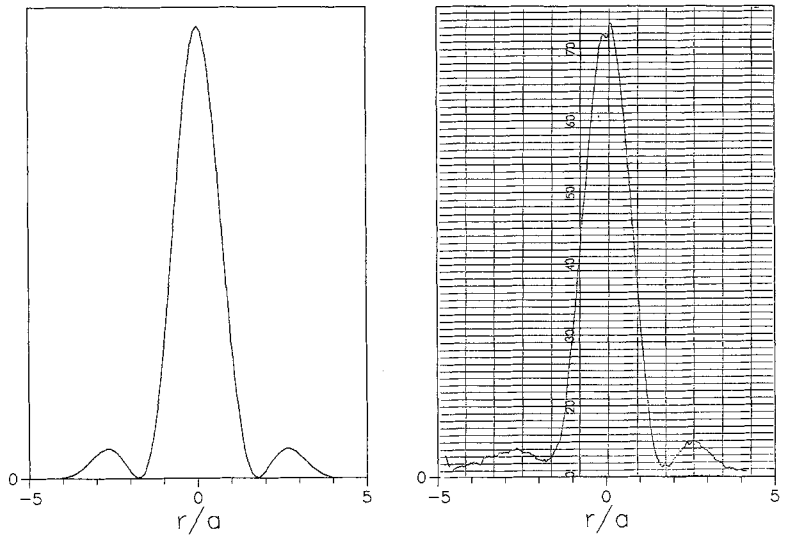

Fig. 11. Calculated and measured intensity profile for front end output beam at a distance of 59 cm from the resonator

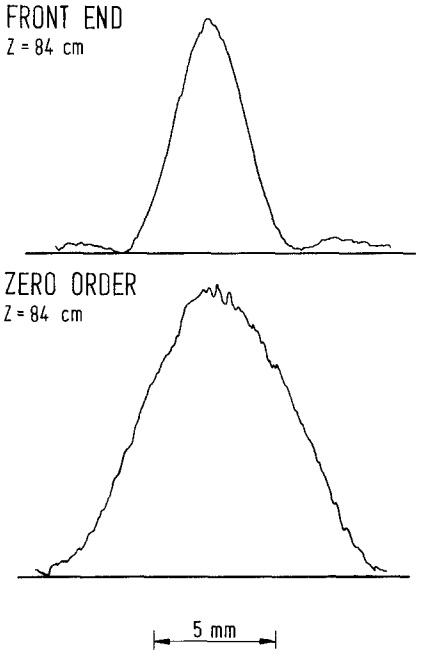

Fig. 13. Comparison of front end beam profile and zero order beam profile, both recorded at a distance of 84 cm from the resonator

tion in a circular aperture with a radius of 90% of the waveguide radius, but with significantly stronger side lobes. In Fig. 10 we show the HWHM point of the central peak, the radius of the zero intensity ring, and the radius of the intensity maximum of the first ring, as a function of distance from the output coupler. All points are located on straight lines which extrapolate to a point located about 2 cm inside the waveguide. Figure 11 compares the measured and calculated profile at a distance of 59 cm from the output coupler, using only a single adjustable amplitude factor. The good agreement obtained for the strength of the side lobes and for the beam width, shows that the model provides excellent predictions for the far field intensity pattern.

A different way of coupling out of the resonator is through the zero order reflection from the grating. At this position, the intensity profile is very different from that at the output mirror, and the same holds for the far field intensity profile, which according to calculations develops as shown in Fig. 12. In Fig. 13 we compare the measured intensity profiles of the two output beams at a distance of 84 cm from the resonator, and we find that the overall width of the zero order beam is more than twice as large as that of the front end beam.

5. Higher Order Modes

Higher order modes were studied for $l_g = 0.209$, where a number of different modes may oscillate over a range of d_2 values. Calculated far field intensity profiles for the four modes considered in Sect. 4.2 are shown in Fig. 14. Experimentally, the different modes were selected by reducing the pressure in the laser to 30 Torr in order to narrow the gain width, and tuning the resonator length to the appropriate photoacoustic peak.

The condition for oscillation at the center of the gain profile is that at the corresponding frequency, the phase change of the field during a double pass of the resonator equals an integral number of 2π. Denoting the phase of the eigenvalue as ϕ, this condition is expressed as

$$2kL + \phi = 2\pi q . \tag{22}$$

Thus, for a given longitudinal order q, eigensolutions with different ϕ will oscillate at different values of resonator length L, and the relative phases can be measured directly from the relative location of the photoacoustic absorption in a resonator length scan, with one full period corresponding to 2π.

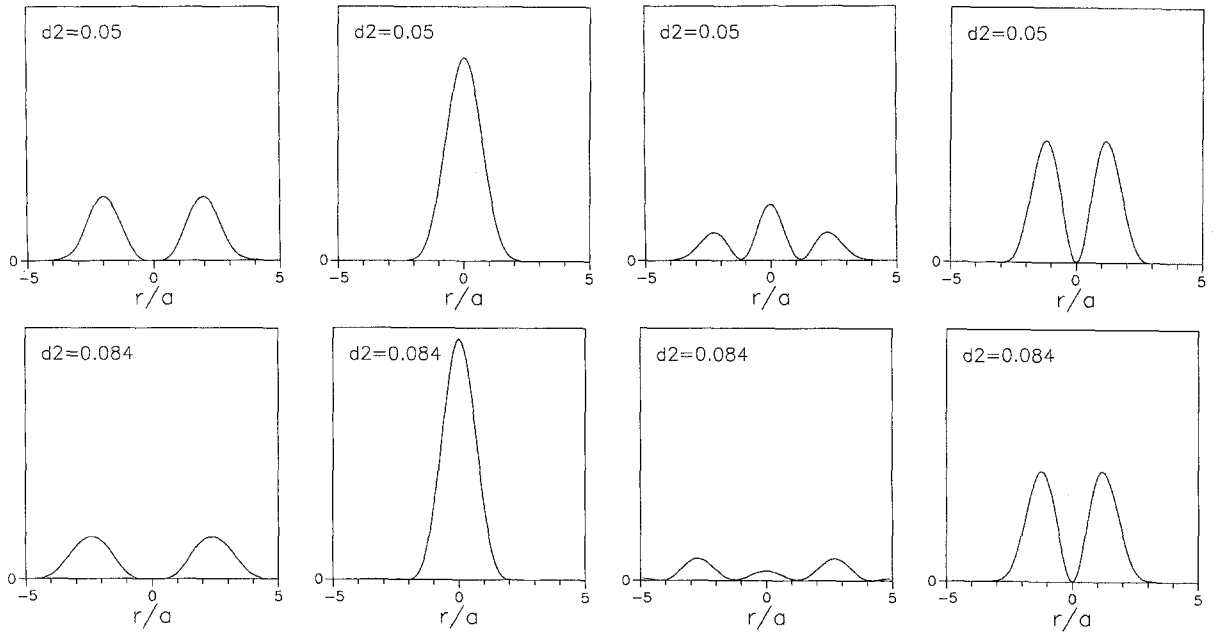

Fig. 14. Calculated normalized far field intensity profiles for the four modes considered in Figs. 6 and 7, evaluated at a distance of 45 cm from the output coupler

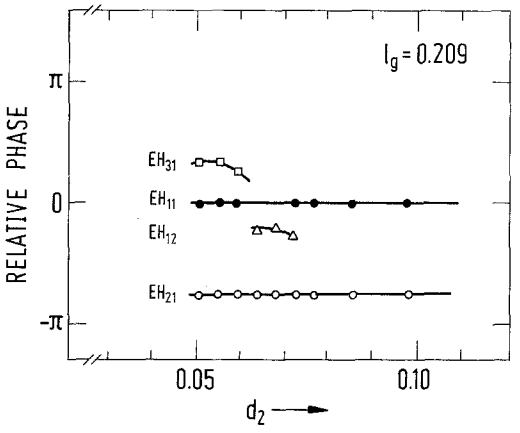

Fig. 15. Observed relative phases of the four modes considered in Figs. 6 and 7. The free spectral range is equivalent to 2π

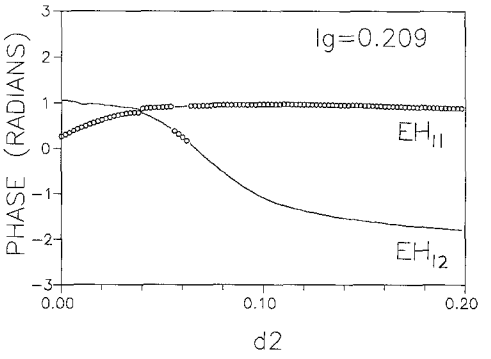

Fig. 17. Calculated relative phase of EH_{11} and EH_{12} mode. Heavy lines indicate the mode with lowest loss

Figure 15 shows for a range of d_2 values the relative phases of the observed modes, measured relatively to the phase of the fundamental mode, and the corresponding recorded intensity profiles are shown in Fig. 16. The EH_{31} doughnut mode appears reasonably clean at $d_2 = 0.0496$, whereas at larger d_2 values the central peak indicates some admixture of the fundamental EH_{11} mode. The phase difference between the two modes is $\leqq \pi/3$, and this is not enough to ensure complete separation. The EH_{11} mode is observed over the entire range of d_2 values, except between 0.06 and 0.07. It is dominated by the central peak, and the side lobes, which are relatively strong at low d_2, presumably reflect a contribution from EH_{12}. Theoretically, only very small side lobes are expected, and at high d_2, where the EH_{12} contribution vanishes, the observations agree with this prediction. In the intermediate range a different mode pattern occurs, with comparable intensity in a central peak and a ring. This is the pattern expected for the EH_{12} mode, and the d_2 range over which it is observed, corresponds well with the range in which the EH_{12} loss dips down below the EH_{12} loss. As a further corroboration, we show in Fig. 17 the calculated phase of the mode with lowest loss, and it is seen that a phase jump of the right sign and magnitude is expected in this range. Also, it will be noted that the theoretical prediction of a rapid shift of intensity away from the central peak and into the ring, with increasing d_2, is well supported by the experiment. Finally, over the entire range of d_2 values, the EH_{21} doughnut mode is observed, and we see that the ring diameter is smaller than for the EH_{31} doughnut, in agreement with expectations. Since there is nothing in our theoretical model which couples modes with a different number of azimuthal nodal planes, it is not possible to predict the relative phases of such modes.

Although the various modes are well enough separated that their identity can be inferred from the intensity pattern, the presence of a finite intensity at the center of the doughnut modes indicate a residual contribution from the EH_{11} mode. This contribution will lead to a reduction of the ring diameter, and it is therefore not too surprising that the measured diameters are 20% smaller than calculated. A similar situation exists for the EH_{11} mode at low d_2, where the EH_{12} contribution leads to a central peak which is also about 20% narrower than predicted for the pure fundamental mode.

6. Conclusion

In the previous sections we have extended the treatment of hollow dielectric waveguide lasers with free space regions and flat mirrors, introduced by [8], to cover the most important higher order modes, and in this way we have identified regions of high mode discrimination in the parameter space. A study of Fig. 3 shows that any attempt at achieving large single mode tunability in a waveguide laser with the reflectors very close to the waveguide, will meet with difficulties, since at least four different modes have total losses well below 10% per double pass. On the

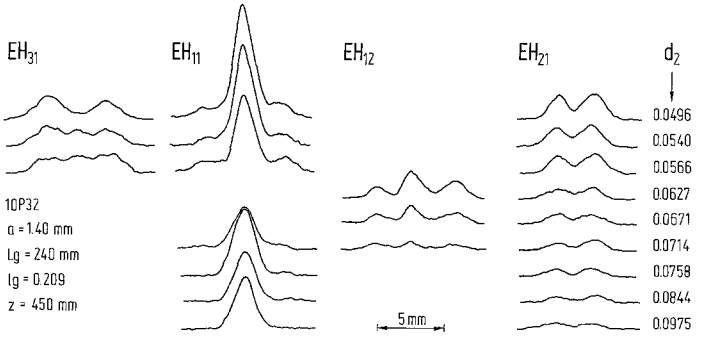

Fig. 16. Measured far field intensity profiles corresponding to Fig. 14

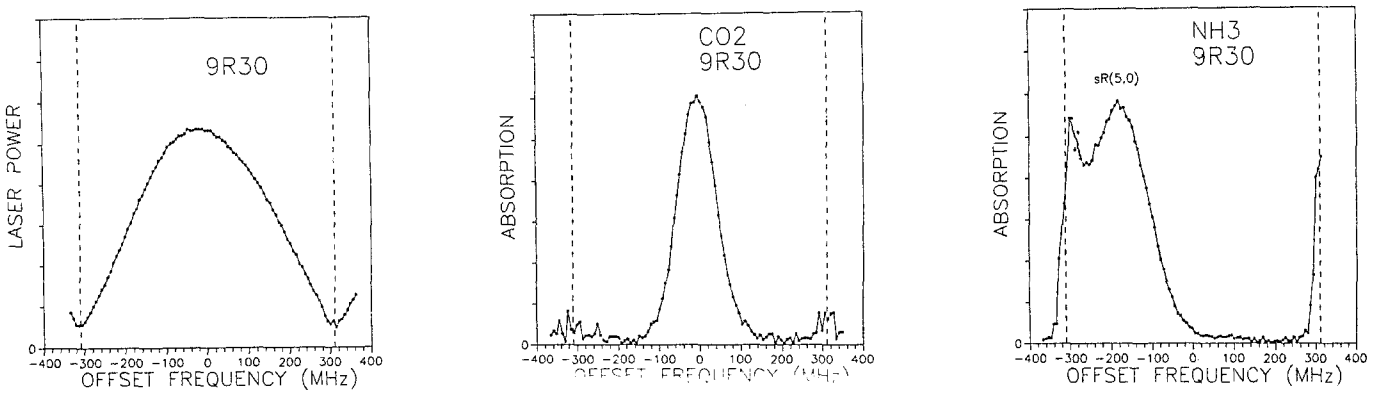

Fig. 18a–c. Spectroscopic test of single line and single mode tuning over 620 MHz in 9*R*30. Photoacoustic signals are for CO_2 (**b**), and for the $sR(5, 0)$ absorption line of NH_3, located at -190 MHz with respect to the CO_2 line center (**c**). Part of the $sR(5, 1)$ line centered at -350 MHz is also seen

other hand, by varying the separation between one of the reflectors and the waveguide, it is possible to find a configuration where the fundamental mode loss is less than 5%, whereas the first higher order mode has more than 50% loss per double pass, and this laser will be totally immune to higher order mode oscillation.

The calculated magnitude of the coupling losses is compared with experiments by studying the output power of CO_2 lasers for a wide range of resonator configurations. It is noteworthy that quantitative agreement is obtained both for the structure in the D_2 dependence, and for the maximum value of D_2 for which the lasers can oscillate, despite the fact that the lasers differ by up to a factor of 2 in active length, and almost a factor of 3 in active volume. Four different higher order modes are included in the analysis, and three of them have been identified experimentally.

The intensity profile inside and outside the resonator has been studied for the fundamental mode, and we find that the profile changes dramatically with position in the resonator. A logical consequence is that the extra cavity profile will also depend strongly on the choice of output plane. In our lasers we could choose front end outcoupling through a dielectric mirror, or zero order outcoupling from the grating, and for the configuration studied, the two beams are both non-gaussian, and very different both as far as shape and width are concerned. Again, however, both shape and width is accurately predicted by the calculations.

The far field pattern for three higher order modes was studied experimentally and theoretically. For these modes the qualitative agreement was good, but the measured beam width for all of them was about 20% smaller than predicted. This may be a consequence of the fact that none of them can experimentally be perfectly separated from the fundamental mode. However, it cannot be ruled out that the truncation to two waveguide modes and five free space modes for fields with azimuthal nodal planes is too brutal.

The overall conclusion is that the model used by [8] and extended as discussed above, is capable of explaining most essential features of hollow dielectric waveguide lasers, and of providing quantitatively correct predictions. By a suitable choice of design parameters, single line and single mode tuning can be achieved over a wide frequency range, even in the densest regions of the CO_2 laser spectrum. As an illustration we have chosen an example from the high-J region of the 9*R* band, and Fig. 18 shows a scan over 620 MHz in the 9*R*30 line, allowing the observation of a strong absorption in NH_3, centered 190 MHz below the CO_2 line center.

One feature which cannot be explained, is the relative phase shift between eigenmodes of different azimuthal symmetry, since the model does not allow for any interaction between such modes. However, in view of the large variations of the beam profiles with position in the resonator, it is plausible that the relative phases are determined by the requirement that the spatial overlap between different eigenmodes is minimized.

Although the motivation for this study was the desire to achieve a good understanding of waveguide lasers, it is conceivable that the theory might be relevant to conventional open structure lasers as well. A typical cw CO_2 laser has a 100 cm discharge tube with 10 mm diameter, and this configuration corresponds to a normalized waveguide length of $l_g = 0.067$ at 10.6 μm. Inspection of Table 2 shows that an EH_{11}/EH_{13} loss minimum is expected around $l \simeq 0.091$, corresponding to a resonator length of 135 cm. Since the discharge tube is deliberately chosen large enough that a fundamental $TEM_0^{(0)}$ mode can propagate with low diffraction losses, it follows that a waveguide mode will utilize the gain medium more efficiently, and unless an intra cavity aperture is used, it is quite likely that the laser will prefer oscillating in a waveguide mode. For quantitative considerations one must of course take into account that open structure resonators use curved mirrors, whereas the theory, as developed above, applies to resonators with flat mirrors. Another potential area of relevance is optically pumped far infrared lasers. For cw lasers the much lower operating pressure in conjunction with the reduced Doppler width means that the gain width is usually much smaller than the free spectral range. Single mode operation can therefore be achieved without relying on loss discrimination, by just choosing the appropriate resonator length. For high power pulsed lasers, however, the situation is

different, and here the loss discrimination may be a necessary ingredient.

References

1. T.J. Bridges, E.G. Burkhardt, P.W. Smith: Appl. Phys. Lett. **20**, 403–405 (1972)
2. R.L. Abrams: Appl. Phys. Lett. **25**, 304–306 (1974)
3. E.A.J. Marcatili, R.A. Schmeltzer: Bell. Syst. Tech. J. **43**, 1783–1809 (1964)
4. J.J. Degnan, D.R. Hall: IEEE J. QE-**9**, 901–910 (1973)
5. F.P. Roullard III, M. Bass: IEEE J. QE-**13**, 813–819 (1977)
6. M. Lyszyk, F. Herlemont, J. Lemaire: Optics Commun. **36**, 327–330 (1981)
7. R.E. Jensen, M.S. Tobin: Appl. Phys. Lett. **20**, 508–510 (1972)
8. R. Gerlach, D. Wei, N.M. Amer: IEEE J. QE-**20**, 948–963 (1984)
9. W.W. Rigrod: J. Appl. Phys. **36**, 2487–2490 (1965)
10. R.L. Abrams: IEEE J. QE-**8**, 838–843 (1972)
11. F. Tang, J.O. Henningsen: IEEE J. QE-**22**, 2084–2087 (1986)
12. F. Tang, J.O. Henningsen: Appl. Phys. B **44**, 93–98 (1987)